Diagn Interv Radiol 2020; 26:22–27

GENERAL RADIOLOGY

ORIGINAL ARTICLE

The impact of irreversible image data compression on post-processing algorithms in computed tomography

Daniel Pinto dos Santos
Conrad Friese
Jan Borggrefe
Peter Mildenberger
Aline Mähringer-Kunz
Roman Kloeckner

PURPOSE
We aimed to evaluate the influence of irreversible image compression at varying levels on image post-processing algorithms (3D volume rendering of angiographs, computer-assisted detection of lung nodules, segmentation and volumetry of liver lesions, and automated evaluation of functional cardiac imaging) in computed tomography (CT).

METHODS
Uncompressed CT image data (30 angiographs of the lower limbs, 38 lung exams, 20 liver exams and 30 cardiac exams) were anonymized and subsequently compressed using the JPEG2000 algorithm with compression ratios of 8:1, 10:1, and 15:1. Volume renderings of CT angiographies obtained from compressed and uncompressed data were compared using objective and subjective measures. Computer-assisted detection of lung nodules was performed on compressed and uncompressed image data and compared with respect to diagnostic performance. Segmentation and volumetry of liver lesions as well as measurement of ejection fraction on cardiac studies was performed on compressed and uncompressed datasets; differences in measurements were analyzed.

RESULTS
No differences could be detected for the 3D volume renderings and no statistically significant differences in performance were found for the computer-assisted detection algorithm. Measurements in volumetry of liver lesions and functional cardiac imaging showed good to excellent reliability.

CONCLUSION
Irreversible image compression within the limits proposed by the European Society of Radiology has no significant influence on commonly used image post-processing algorithms in CT.

Over the last decades, radiology has evolved from analogue film-based workflows to full digitization. Radiological images are stored in a picture archiving and communication system (PACS) and viewed on high-resolution computer displays. Parallel to these developments, technical advances such as the introduction of multidetector computed tomography (CT) or spectral CT and magnetic resonance imaging (MRI) capable of complex examinations such as 4D functional imaging have led to a significant increase in the size and number of digital images (1).

For legal reasons, all radiology departments must store all images and related data for a defined period of time, often up to ten years and more. Therefore, intelligent management of storage and network capacity has become a major issue. Although costs for storage solutions have significantly decreased over the last few years, thus mitigating the potential economic burden, network bandwidth remains a problem, especially when considering tele-radiological applications.

One possible solution to address these issues is image compression. Reversible image compression, e.g., using entropy encoding and thus reducing redundancy of information, allows for minimizing the data volume without any loss of information. Irreversible compression, in contrast, uses additional methods such as undersampling, transformation and quantization techniques to further reduce data volume (2). However, the benefit

From the Department of Radiology (D.P.d.S. ✉ *daniel.pinto-dos-santos@uk-koeln.de*, J.B.), University Hospital Cologne, Cologne, Germany; Department of Diagnostic and Interventional Radiology (D.P.d.S., C.F., P.M., A.M.K., R.K.), University Medical Center of the Johannes Gutenberg University Mainz, Mainz, Germany; Department of Internal Medicine (C.F.), St. Hildegardis Hospital, Cologne, Germany.

Received 27 December 2018; revision requested 06 February 2019; last revision received 11 June 2019; accepted 21 June 2019.

Published online 6 December 2019.

DOI 10.5152/dir.2019.18245

You may cite this article as: Pinto dos Santos D, Friese C, Borggrefe J, Mildenberger P, Mähringer-Kunz A, Kloeckner R. The impact of irreversible image data compression on post-processing algorithms in computed tomography. Diagn Interv Radiol 2020; 26:22–27.

of further reducing file sizes comes at the price of losing image information. Most methods for irreversible image compression attempt to only discard information that is not noticeable to the human observer, thus providing "visually lossless" image compression at higher compression ratios than those being possible with reversible image compression.

Various radiological societies have published recommendations for the use of irreversible image compression in DICOM images, such as the Royal College of Radiologists (RCR), the German Roentgen Society (DRG), the Canadian Association of Radiologists (CAR), and the European Society of Radiology (ESR) (3–6). These recommendations suggest the use of either JPEG or JPEG2000, which were both introduced by the Joint Photographic Experts Group and are widely used. In this context, "compression ratio" indicates the amount of reduction in data volume; it is the quotient of the original image size and the compressed image size. For the use of image interpretation in radiology, acceptable compression ratios should be below the "visually lossless" threshold. Recommendations range from 5:1 for head CT scans to 30:1 for conventional chest X-rays (3–6).

The abovementioned recommendations are based on available evidence suggesting no relevant reduction in diagnostic accuracy for irreversibly compressed images compared with reversibly compressed images. However, only little data is available on whether irreversible image compression poses relevant problems in advanced image post-processing workflows, such as volume rendering or segmentation.

To address this lack of evidence, the aim of this study was to assess the impact of irreversible image compression on different advanced post-processing algorithms commonly used in CT.

Main points

- Commonly used post-processing algorithms are not influenced by image compression.
- Image compression as proposed by the European Society of Radiology is safe for image post-processing.
- Further studies are needed to evaluate impact of image compression on machine learning and radiomics.

Methods

For the purpose of this study four commonly used post-processing techniques were chosen to assess the impact of image compression: a) 3D volume rendering of CT angiographs of the lower extremities, b) computer-assisted detection (CAD) of lung nodules in chest CT, c) automatic segmentation of liver lesions in abdominal CT, and d) functional measurement of ejection fraction in electrocardiogram (ECG)-gated cardiac CT.

All image data used in this study were obtained from clinical routine at our institution. Datasets were anonymized and analyzed retrospectively. Therefore, approval and informed consent were not necessary and specifically waived by the local institutional review board.

Prior to the beginning of this study image data had been stored in the institutions' PACS (Cerner MultiMedia Archive) in the standard DICOM format using no or only fully reversible image compression methods. After retrieval and anonymization, image data was compressed on a dedicated workstation using the JPEG2000 algorithm (ISO/IEC 15444-1:2000) with three different compression ratios: 8:1, 10:1, and 15:1. These compression ratios were based on the recommendations of the ESR and the DRG and are therefore within the limits considered suitable for clinical routine. We chose JPEG2000 over JPEG, since it is not restricted to a maximum of 8-bit depth and supports features like streaming, which make it more practical in clinical routine. In this study, we focused on CT examinations only, since these account for a major part of the data produced in clinical routine and are most often used for image post-processing.

All images were acquired on a 64-slice Brilliance CT scanner according to the institution's standard operating procedures (Philips Medical Systems). To maximize the potential effect of irreversible image compression on post-processing, we chose to only include thin-slice CT images (1 mm slice thickness), as these have been shown to be less tolerant to image compression (7).

3D volume rendering of CT angiographs of the lower extremities

A total of 30 consecutive CT angiographs of the lower extremities were included for this study part. Volume renderings were reconstructed from original and irreversibly compressed data with TeraRecon Aquarius (TeraRecon) using fixed reconstruction settings. Screenshots of these renderings were taken in previously determined standardized positions and were then subjectively compared for noticeable differences by two board-certified radiologists experienced in cardiovascular imaging (Fig. 1). Readers were presented pairs of renderings obtained from uncompressed and compressed data in a randomized order. They were blinded to whether the image was compressed or not and to the compression ratios used. If the readers noticed subjectively discernible visual differences, they were asked to indicate which image was obtained from compressed data. Additionally, peak signal-to-noise ratio (PSNR) and high dynamic range visual difference predictor (HDR-VDP) were calculated for renderings from original and compressed data. Whereas the PSNR is a purely mathematical description of difference between two images, the HDR-VDP tries to mimic human perception, identifying pixels that might be perceived as different with certain probabilities (8, 9).

Computer-assisted detection of lung nodules

For this part of the study, 38 consecutive chest CT studies were included where one

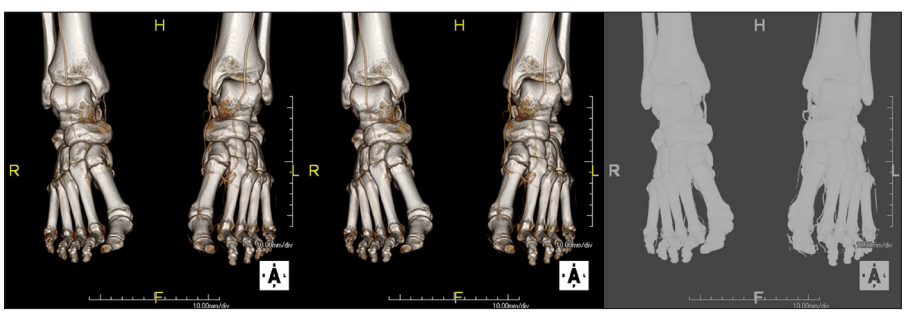

Figure 1. Example of 3D volume rendering of an angiograph of the lower extremities. Screenshot obtained from original dataset is shown on the left, image obtained from the 15:1 compressed dataset in the middle. Right image is the result of the HDR-VDP algorithm, no pixels were marked as detectable differences for both probability settings.

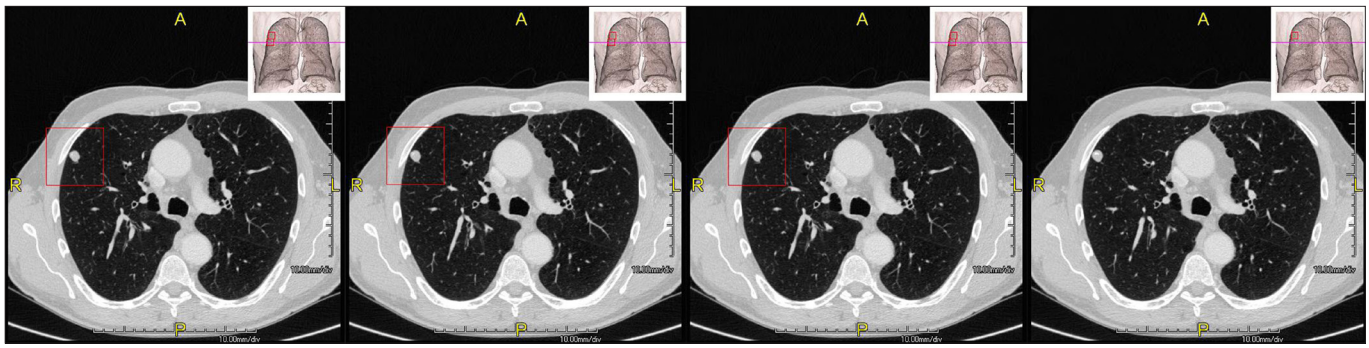

Figure 2. Example of the results of the CAD algorithm. Images depict results from original, 8:1, 10:1, and 15:1 compressed images. Interestingly, in this example the nodule is not detected in the 15:1 compressed dataset. In other cases, nodules that were detected on compressed datasets were not detected in the uncompressed.

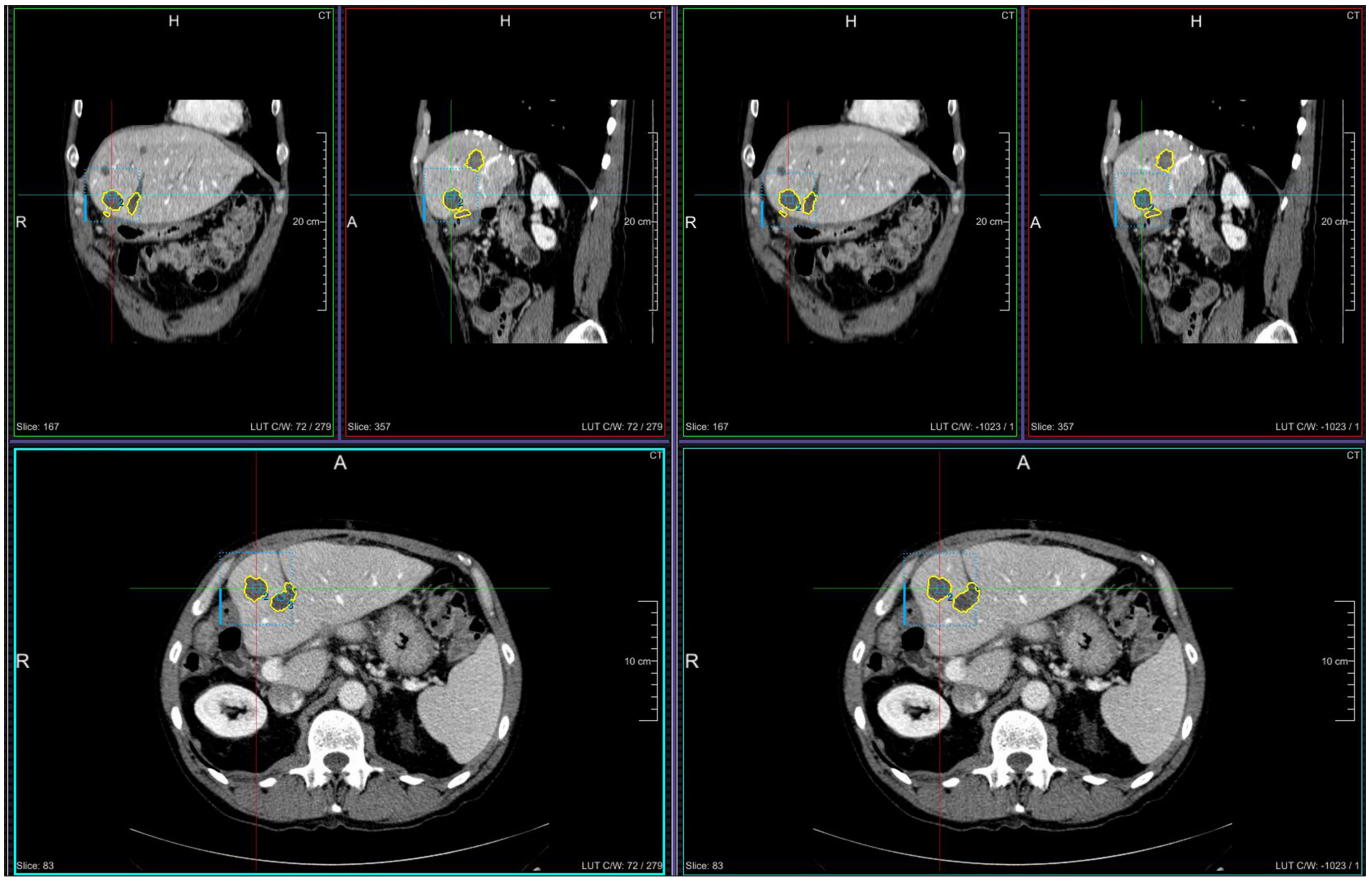

Figure 3. Example for the semi-automated segmentation and volumetry of liver lesions *(yellow circles)* The result on the right was produced with the original dataset, while the compressed dataset with the corresponding results is shown on the left. Visually, no differences can be perceived. Quantitative results also showed no significant difference.

or more incidental lung nodules between 4 and 10 mm had been reported. All CT scans were performed in different patients. CAD was performed on original and compressed data using TeraRecon Aquarius (TeraRecon). The CAD algorithm assigns each finding a score between 0 and 1, with 1 representing maximum certainty of a lung nodule. For the purpose of this study, findings with a CAD score above 0.4 were included as a detected nodule. We defined a consensus reading by two radiologists experienced in chest imaging as the reference standard, yielding a total of 134 nodules. Accordingly, all CAD findings from the different datasets were either classified as true or false findings (e.g., blood vessel identified as a nodule) (Fig. 2).

Automated volumetric analysis of liver lesions

For this part of the study, 20 consecutive abdominal CT studies with a total of 59 hypodense liver lesions in portal venous phase were included. Again, all CT scans were performed in different patients. Semi-automated segmentation and volumetry of liver lesions were performed using a prototype application (MeVis Medical Solutions AG). After initial selection of a lesion on the uncompressed dataset, measurements were performed automatically. Subsequently, the segmentation seed point was copied to the same location on the

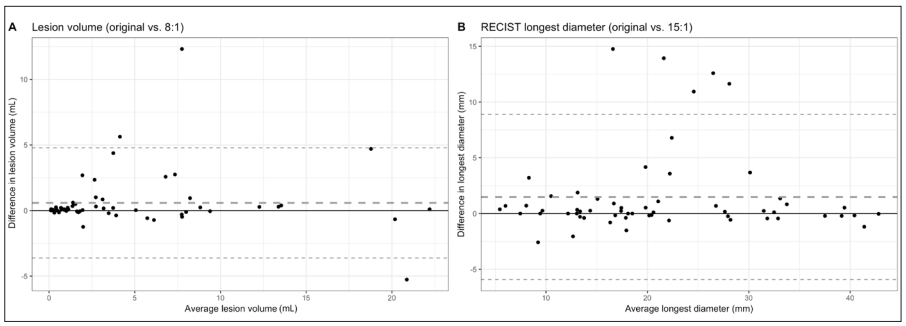

Figure 4. Example of two Bland-Altmann plots for the comparison of measurements from semi-automated segmentation and volumetry of liver lesions (*dashed lines* represent mean of difference and limits of agreement).

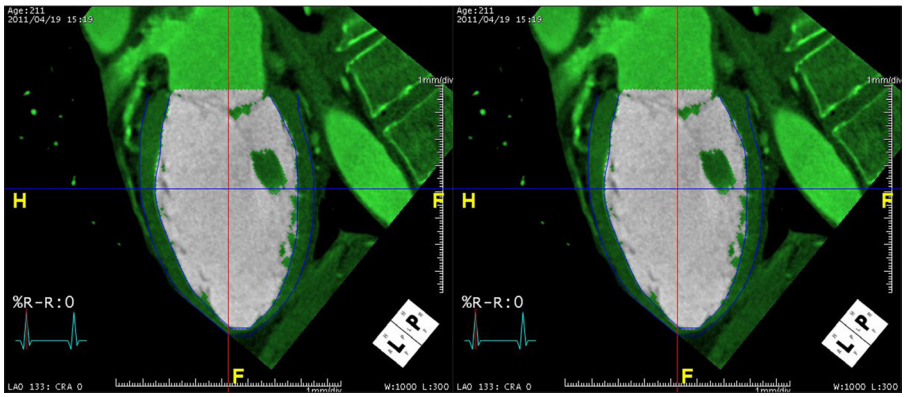

Figure 5. Example for the automated evaluation of functional cardiac imaging: masked image *(green)*, left ventricular myocardium *(blue lines)*, left ventricular cavity *(clear areas)*. The right part of the image shows the segmentation results in the original dataset, while the compressed dataset with the corresponding results is shown on the left.

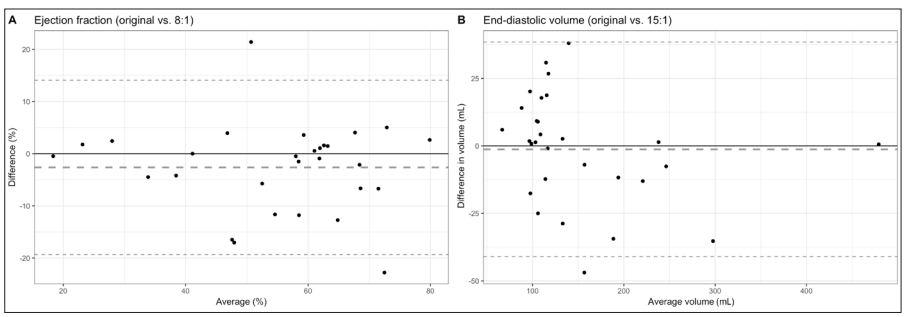

Figure 6. Example of two Bland-Altmann plots for the comparison of measurements from automated evaluation of functional cardiac imaging (*dashed lines* represent mean of difference and limits of agreement).

Table 1. Results for comparison of volume renderings using PSNR and HDR-VDP

	8:1	10:1	15:1
PSNR original vs.			
Median (quartiles), dB	49.89 (48.84–50.94)	49.61 (48.57–50.80)	48.89 (47.98–49.98)
HDR-VDP (%)			
0.95 probability / 0.75 probability	<0.001 / <0.001	<0.001 / <0.001	<0.001 / <0.001

PSNR, peak signal-to-noise ratio; HDR-VDP, high dynamic range visual difference predictor.

compressed datasets using the software's dedicated tool with no further user input. Volume, equivalent spherical diameter, and measurements according to the Response Evaluation Criteria in Solid Tumors (RECIST) and WHO criteria were recorded (Fig. 3).

Functional cardiac imaging

For the fourth part of the study, we included 30 consecutive cardiac CT studies acquired with retrospective ECG-gating allowing for functional assessment. Each study included 10 reconstructed series in different phases of the cardiac cycle. Measurements were performed with TeraRecon Intuition (TeraRecon). After locating the left ventricle and the level of the aortic valve as well as adjusting thresholds in the uncompressed dataset, the software allowed for automatic calculation of end-diastolic and end-systolic left ventricular volume as well as calculation of ejection fraction (Fig. 5). All settings were subsequently transferred to the compressed datasets. Again, differences in measurements were analyzed using intraclass correlation coefficients (ICC) (10).

Statistical analysis

Statistical analysis was carried out using the software SPSS for macOS, version 25.0 (IBM Corp.). Differences in classification of the CAD algorithms were evaluated using the McNemar test. Differences in measured numerical values for liver lesions and functional cardiac imaging were analyzed using intraclass correlation coefficients (ICC, two-way mixed, single measures consistency – ICC(3,1) in Shrout and Fleiss convention) (10).

Results

When comparing screenshots of 3D volume renderings of CT angiographies of the lower extremities reconstructed from original and compressed datasets, a slight decrease in average PSNR was measured (49,89 dB for original vs. 8:1, 49,61 dB original vs. 10:1, 48,89 dB original 15:1) (Table 1). HDR-VDP classified 0% of all pixel as detectable differences for both probability settings ($P = 0.95$ and $P = 0.75$) (Table 1). As for the subjective reading, the first reader could not identify any differences for any comparison, whereas the second reader suggested there were minor visual differences in two out of the 90 presented pairwise comparisons. For these, in one case the rendering from the uncompressed dataset was thought to be produced from compressed data, whereas in the other case the reader correctly identified the rend ering from the irreversibly compressed dataset.

In detection of lung nodules, the CAD algorithm was applied to all datasets (uncompressed and the three compressed).

Table 2. Contingency tables for the comparison of computer aided detection (CAD) of lung nodules

		Radiologists' consensus	
		No nodule	Nodule
CAD (original)	No nodule	0	49
	Detected nodule	15	85
CAD (8:1)	No nodule	0	48
	Detected nodule	20	86
CAD (10:1)	No nodule	0	51
	Detected nodule	18	83
CAD (15:1)	No nodule	0	55
	Detected nodule	18	79

No significant differences were found ($P_{8:1} = 0.21$, $P_{10:1} = 1.00$, $P_{15:1} = 0.66$). The radiologists' consensus reading identified a total of 134 true nodules. CAD showed comparable performance across all datasets with a sensitivity of 63% in the original dataset and 64%, 62%, and 59% for 8:1, 10:1, and 15:1 compressed datasets.

Table 3. ICC and mean difference / limits of agreement for the comparison of semi-automated segmentation and volumetry of liver lesions (95% confidence interval)

	$ICC_{8:1}$ / mean difference and limits of agreement	$ICC_{10:1}$ / mean difference and limits of agreement	$ICC_{15:1}$ / mean difference and limits of agreement
Lesion volume (mL)	0.96 (0.93–0.97) 0.58 (-3.62–4.78)	0.96 (0.94–0.98) 0.62 (-3.19–4.43)	0.96 (0.93–0.97) 0.52 (-3.83–4.88)
Equivalent spherical diameter (mm)	0.96 (0.94–0.97) 1.07 (-4.69–6.84)	0.96 (0.94–0.98) 1.06 (-4.35–6.49)	0.95 (0.93–0.97) 1.15 (-5.11–7.41)
Longest diameter (mm) (RECIST)	0.96 (0.94–0.98) 1.46 (-5.48–8.41)	0.97 (0.95–0.98) 1.37 (-4.71–7.46)	0.96 (0.93–0.97) 1.48 (-5.91–8.88)
Diameter (mm) (WHO)	0.95 (0.92–0.97) 0.84 (-5.77–7.46)	0.96 (0.94–0.97) 0.71 (-5.09–6.49)	0.95 (0.92–0.97) 1.07 (-5.35–7.50)

ICC, intraclass correlation coefficient; RECIST, response evaluation criteria in solid tumors; WHO, World Health Organization.

Table 4. ICC for the comparison of assessment of functional cardiac imaging (95% confidence interval)

	$ICC_{8:1}$ / mean difference and limits of agreement	$ICC_{10:1}$ / mean difference and limits of agreement	$ICC_{15:1}$ / mean difference and limits of agreement
Ejection fraction	0.95 (0.90–0.98) -2.63 (-19.33–14.07)	0.89 (0.78–0.95) -2.47 (-17.48–12.53)	0.92 (0.82–0.96) -2.58 (-18.08–12.92)
End-diastolic volume	0.97 (0.95–0.99) -3.55 (-45.48–38.36)	0.96 (0.92–0.98) 1.22 (-24.83–27.28)	0.95 (0.89–0.97) -1.27 (-41.06–38.51)
End-systolic volume	0.98 (0.96–0.99) -2.04 (-31.41–27.32)	0.98 (0.96–0.99) 1.13 (-17.73–19.99)	0.97 (0.93–0.98) -0.61 (-31.07–29.83)

ICC, intraclass correlation coefficient.

On the original dataset a total of 100 lung nodules were identified by the CAD algorithm, while in the compressed datasets 106, 101, and 97 nodules were identified (8:1, 10:1, and 15:1, respectively). Comparing all identified nodules from all CAD results a total of 158 distinct findings were indicated by the CAD software. These findings were then compared to the 134 nodules identified by radiologists' consensus reading (Table 2).

In the uncompressed dataset, the CAD algorithm had a total of 100 findings, of which only 85 were true positives. The remaining 49 true nodules were missed, while 15 findings were false positives. This led to a sensitivity of 63% in the uncompressed dataset. Comparable results were found for the compressed datasets although there was considerable variability as to which individual findings were identified on the respective datasets. There was no significant difference in diagnostic performance when comparing accuracy between CAD on uncompressed and compressed data ($P_{8:1} = 0.21$, $P_{10:1} = 1.00$, $P_{15:1} = 0.66$).

Measurements of the segmented liver lesions in the compressed datasets showed consistently excellent reliability with ICCs ranging between 0.95 and 0.97 when compared with measurements in the uncompressed dataset (Table 3, Fig. 4). Mean volumes and RECIST longest diameters were 4.88±5.60 mL / 21.89±9.99 mm for the original dataset, 4.29±5.58 mL / 20.42±9.69 mm for 8:1 compression ratio (mean difference to original: 0.58±2.14 mL ≈ 11.9% / 1.46±3.54 mm ≈ 6.7%), 4.26±5.44 mL / 20.51±9.79 mm for 10:1 compression ratio (mean difference to original: 0.61±1.94 mL ≈ 12.6% / 1.37±3.10 mm ≈ 6.2%) and 4.35±5.90 mL / 20.40±9.82 mm for 15:1 compression ratio (mean difference to original: 0.52±2.22 mL ≈ 10.7% / 1.48±3.77 mm ≈ 6.7%).

In the evaluation of functional cardiac imaging, measurements showed consistently good to excellent reliability with ICCs ranging between 0.89 and 0.98 for all comparisons between the respective compressed datasets and the uncompressed dataset (Table 4, Fig. 6). Mean ejection fraction, end-diastolic volume and end-systolic volume were 53.65%±15.57%, 149.24±81.29 mL and 74.70±74.69 mL for the original dataset, 56.28%±16.37%, 152.79±93.45 mL, 76.74±84.69 mL for 8:1 compression ratio, 56.12%±17.48%, 148.01±84.39 mL, 73.56±75.30 mL for 10:1 compression ratio and 56.23±16.47%, 150.51±86.88 mL, 73.31±74.40 mL for 15:1 compression ratio.

Discussion

Several studies have provided evidence that irreversible image compression can safely be used in the context of image interpretation (11). Consequently, recommendations have been published on which compression method and compression ratio to use without negatively affecting diagnostic accuracy (3–6). Although the cost for data storage might not be the biggest issue nowadays, in settings where large amounts of images need to be transferred in little time with limited network bandwidth, irreversible image compression could considerably speed up data transfer. Kim et al. (12) implemented JPEG2000 in a tele-radiology solution for emergency care with no significant loss of diagnostic performance.

However, only few studies aimed at assessing the effects of irreversible image compression on image post-processing. Therefore, due to the relative lack of further evidence, it was suggested to only use uncompressed data for further image post-processing. Since then, some authors reported on the influence of irreversible compression on CAD algorithms for lung nodule detection. Raffy et al. (13) found no significant influence of irreversible compression on lung nodule CAD for compression ratios up to 48:1. However, Ko et al. (14) reported that irreversible image compression at a compression ratio of 20:1 significantly influenced computer-assisted measurements of lung nodules. Our results are in line with these findings in that we did not find any significant influence of image compression with regards to the CAD's detection rates.

Nevertheless, the influence of irreversible image compression on other post-processing algorithms has not been reported previously. Our findings indicate that for some of the most commonly used image post-processing workflows in CT, irreversible image compression within the limits recommended by major radiological societies is safe and does not have any negative impact on image post-processing and lesion detection.

Although our results are surprisingly clear, there are some limitations to our study: most importantly, due to the relatively small sample size and limited number of algorithms and clinical use cases, it remains uncertain if they can be generalized or are limited to the presented algorithms only. Moreover, other factors such as radiation dose, lesion size and type, reconstruction filters, and slice thicknesses could have a relevant influence on the results of post-processing algorithms. Just like image compression, such factors need to be considered when comparing measurements at different timepoints. In our small study we found a small bias towards slightly larger measurements in the analysis of liver lesions, therefore it seems advisable to ideally only compare studies with identical parameters for reconstruction filters, slice thickness, and compression settings.

Further studies including a wider variety of algorithms and pathologies, ideally controlled for the aforementioned additional influence factors, are needed to ensure comparable performance on uncompressed and irreversibly compressed data. Another minor limitation to our results in evaluating the image quality of 3D volume renderings is that we only used PSNR and HDR-VDP as objective means to compare the images. Other measures such as the SSIM (structural similarity index) could present slightly different results. Especially with the advent of advanced technologies such as radiomics, deep learning and computer vision the impact of image compression on pattern recognition needs to be investigated (15, 16). However, it seems plausible that irreversible image compression introduces only minor changes to the data and therefore algorithms should be robust enough to tolerate moderate compression within the suggested limits. Nevertheless, with more refined image post-processing workflows becoming widely-used in clinical routine, even small artifacts could possibly influence the respective algorithms. Lastly, we limited our study on the application of irreversible image compression to 2D images. Further research is needed to clarify its impact on volumetric medical data, such as DICOM 3D presentation states (17).

In conclusion, software vendors should take varying degrees of irreversible image compression into account when evaluating a software tool's performance. Radiological societies also need to address the arising question whether original data has to be stored at all or if irreversibly compressed data is just as adequate as the original data.

Conflict of interest disclosure

The authors declared no conflicts of interest.

References

1. Hagland M. Image explosion. In the wake of modality advances, CIOs must please radiologists, store huge amounts of data, and not lose sight of the bottom line. Healthc Inform 2009; 26:27–28.
2. Erickson BJ. Irreversible compression of medical images. J Digit Imaging 2002; 15:5–14. [CrossRef]
3. The Royal College of Radiologists. The adoption of lossy image data compression for the purpose of clinical interpretation. 2010; Available from: https://www.rcr.ac.uk/publication/it-guidance-adoption-lossy-image-data-compression-purpose-clinical-interpretation
4. Loose R, Braunschweig R, Kotter E, et al. Compression of digital images in radiology - results of a consensus conference. Rofo 2009; 188:32–37. [CrossRef]
5. Koff D, Bak P, Brownrigg P, et al. Pan-Canadian evaluation of irreversible compression ratios ("lossy" compression) for development of national guidelines. J Digit Imaging 2008; 22:569–578. [CrossRef]
6. European Society of Radiology (ESR). Usability of irreversible image compression in radiological imaging. A position paper by the European Society of Radiology (ESR). Insights Imaging 2011; 2:103–115. [CrossRef]
7. Woo HS, Kim KJ, Kim TJ, et al. JPEG 2000 compression of abdominal CT: difference in tolerance between thin- and thick-section images. AJR Am J Roentgenol 2007; 189:535–541. [CrossRef]
8. Kim KJ, Kim B, Lee KH, et al. Regional difference in compression artifacts in low-dose chest CT images: effects of mathematical and perceptual factors. AJR Am J Roentgenol 2008; 191:W30–W37. [CrossRef]
9. Kim B, Lee KH, Kim KJ, et al. Prediction of perceptible artifacts in JPEG 2000-compressed chest CT images using mathematical and perceptual quality metrics. AJR Am J Roentgenol 2008; 190:328–334. [CrossRef]
10. Koo TK, Li MY. A guideline of selecting and reporting intraclass correlation coefficients for reliability research. J Chiropr Med 2016; 15:155–163. [CrossRef]
11. Braunschweig R, Kaden I, Schwarzer J, et al. Image data compression in diagnostic imaging: international literature review and workflow recommendation. Rofo 2009; 181:629–636. [CrossRef]
12. Kim DK, Kim EY, Yang KH,et al. A mobile tele-radiology imaging system with JPEG2000 for an emergency care. J Digit Imaging 2010; 24:709–718. [CrossRef]
13. Raffy P, Gaudeau Y, Miller DP, et al. Computer-aided detection of solid lung nodules in lossy compressed multidetector computed tomography chest exams. Acad Radiol 2006; 13:1194–1203. [CrossRef]
14. Ko JP, Chang J, Bomsztyk E, et al. Effect of CT image compression on computer-assisted lung nodule volume measurement. Radiology 2005; 237:83–88. [CrossRef]
15. Lubner MG, Smith AD, Sandrasegaran K, et al. CT texture analysis: definitions, applications, biologic correlates, and challenges. Radiographics 2017; 37:1483–1503. [CrossRef]
16. Kumar V, Gu Y, Basu S, et al. Radiomics: the process and the challenges. Magn Reson Imaging 2012; 30:1234–1248. [CrossRef]
17. Fischer F, Selver MA, Gezer S, et al. Systematic parameterization, storage, and representation of volumetric DICOM data. J Med Biol Eng 2015; 35:709–723. [CrossRef]